HHS Public Access

Author manuscript

*Biosens Bioelectron X*. Author manuscript; available in PMC 2023 October 05.

Published in final edited form as:

*Biosens Bioelectron X*. 2023 September ; 14: . doi:10.1016/j.biosx.2023.100380.

# Smart capsule for monitoring inflammation profile throughout the gastrointestinal tract

**Sarath Gopalakrishnan**[a,b,1], **Rithu Thomas**[a,1], **Sotoudeh Sedaghat**[b,c,1], **Akshay Krishnakumar**[a,b], **Sadid Khan**[d], **Trevor Meyer**[d], **Hans Ajieren**[d], **Sina Nejati**[b,c], **Jiangshan Wang**[b,e], **Mohit S. Verma**[b,e,f], **Pedro Irazoqui**[d], **Rahim Rahimi**[a,b,c,*]

[a]School of Electrical and Computer Engineering, Purdue University, West Lafayette, IN, 47907, USA

[b]Birck Nanotechnology Center, Purdue University, West Lafayette, IN, 47907, USA

[c]School of Materials Engineering, Purdue University, West Lafayette, IN, 47907, USA

[d]Department of Electrical and Computer Engineering, Johns Hopkins University, Baltimore, MD, 21218, USA

[e]Department of Agricultural and Biological Engineering, West Lafayette, IN, 47907, USA

[f]Weldon School of Biomedical Engineering, West Lafayette, IN, 47907, USA

## Abstract

Inflammatory bowel disease (IBD) has become alarmingly prevalent in the last two decades affecting 6.8 million people worldwide with a starkly high relapse rate of 40% within 1 year of remission. Existing visual endoscopy techniques rely on subjective assessment of images that are error-prone and insufficient indicators of early-stage IBD, rendering them unsuitable for frequent and quantitative monitoring of gastrointestinal health necessary for detecting regular relapses in IBD patients. To address these limitations, we have implemented a miniaturized smart capsule (2.2 cm × 11 mm) that allows monitoring reactive oxygen species (ROS) levels as a biomarker of inflammation for quantitative and frequent profiling of inflammatory lesions throughout the gastrointestinal tract. The capsule is composed of a pH and oxidation reduction potential (ORP)



*Corresponding author. School of Electrical and Computer Engineering, Purdue University, West Lafayette, IN, 47907, USA. rrahimi@purdue.edu (R. Rahimi).

[1]Equal contribution.

Declaration of competing interest

The authors declare that they have no known competing financial interests or personal relationships that could have appeared to influence the work reported in this paper.

CRediT authorship contribution statement

**Sarath Gopalakrishnan:** Conceptualization, Methodology, Writing – original draft, Validation. **Rithu Thomas:** Methodology, Software, Data curation, Writing – original draft. **Sotoudeh Sedaghat:** Methodology, Data curation, Writing – original draft. **Akshay Krishnakumar:** Methodology, Data curation, Writing – original draft. **Sadid Khan:** Software, Resources. **Trevor Meyer:** Software, Resources. **Hans Ajieren:** Software, Resources. **Sina Nejati:** Data curation. **Jiangshan Wang:** Methodology, Data curation. **Mohit S. Verma:** Conceptualization, Supervision. **Pedro Irazoqui:** Conceptualization, Supervision. **Rahim Rahimi:** Conceptualization, Methodology, Writing – review & editing, Project administration, Funding acquisition, Supervision.

Appendix A. Supplementary data

Supplementary data to this article can be found online at https://doi.org/10.1016/j.biosx.2023.100380.

sensor to track the capsule's location and ROS levels throughout the gastrointestinal tract, respectively, and an optimized electronic interface for wireless sensing and data communication. The designed sensors provided a linear and stable performance within the physiologically relevant range of the GI tract (pH: 1–8 and ORP: −500 to +500 mV). Additionally, systematic design optimization of the wireless interface electronics offered an efficient sampling rate of 10 ms for long-running measurements up to 48 h for a complete evaluation of the entire gastrointestinal tract. As a proof-of-concept, the capsule the capsule's performance in detecting inflammation risks was validated by conducting tests on in vitro cell culture conditions, simulating healthy and inflamed gut-like environments. The capsule presented here achieves a new milestone in addressing the emerging need for smart ingestible electronics for better diagnosis and treatment of digestive diseases.

**Keywords**

Smart capsule; Ingestible electronics; Inflammatory bowel disease; Oxidation reduction potential; Wireless sensing

## 1. Introduction

Disorders of the human digestive tract can lead to many diseases like gastroesophageal reflux disease, cancer, Inflammatory Bowel Disease (IBD), lactose intolerance, and hiatal hernia ("Digestive diseases: MedlinePlus Medical Encyclopedia," n.d.). Among these disorders, IBD is a condition involving chronic relapsing inflammation of tissues in the gastrointestinal (GI) tract (Zhu and Li, 2012). IBD is mainly classified as ulcerative colitis and Crohn's disease, usually characterized by persistent diarrhea, abdominal pain, rectal bleeding, weight loss, and fatigue (Jain, 2011). Currently, 6.8 million people around the world suffer from IBD (Alatab et al., 2020), whose prevalence rate is expected to increase by a factor of 1.47 by 2030 (Santiago et al., 2022). Although the exact cause of IBD is not fully understood, there has been some evidence that associates IBD with heredity, diet, lifestyle, behavior, and gut microbiota perturbations through antibiotics (Ananthakrishnan, 2015). In a healthy human body, the epithelium, a thin tissue lining the alimentary canal, forms a physical and immunological barrier that prevents direct contact between luminal microbiota and the host immune system (Coskun, 2014). Disruption of this epithelium layer leads to interaction between the mucosal immune system and the microbiota and causes inflammation in the inner lumen of the GI tract (Krishnakumar et al., 2022a; Lechuga and Ivanov, 2017). The immune system reacts to microbial invasion through the recruitment of neutrophils to the site of inflammation to recognize pathogens and kill them in three ways – phagocytosis, degranulation, and NETosis, of which the latter is commonly observed in IBD patients (Rosales, 2018). NETosis is the formation of neutrophil extracellular traps (NETs) triggered by degranulation of the leukocyte (Brinkmann et al., 2004). This process releases antimicrobial agents, such as myeloperoxidase (MPO), which mediate the production of reactive oxygen species (ROS).

Additionally, during NETosis, neutrophils release alarming proinflammatory chemokines, such as calprotectin, during inflammation. While the neutrophil action is regulated in

proportion to the severity of microbial invasion under normal circumstances, IBD patients have a deregulated immune response which leads to an aberrant level of NETosis at the site of microbial invasion. Excessive and prolonged NETosis at the site of microbial invasion leads to chronic inflammation accompanied by the overproduction of associated biomarkers such as ROS, MPO, and calprotectin.

Although immunosuppressive drugs have been widely used to deescalate inflammation, IBD has demonstrated a high-risk relapse rate of 28.7% within one year of remission (Zhang et al., 2020). The severity and relapsing nature necessitate long-term treatment and continuous monitoring of the inflamed sites throughout the GI tract of the patient. To effectively detect IBD and prevent risks of relapses, bowel damage must be assessed correctly, and prognostic factors incorporated, which calls for frequent monitoring of the GI tract and infective lesions throughout the treatment (Roda et al., 2020).

To detect elevated levels of biomarkers, fecal analyses using C-reactive protein (CRP) and fecal Calprotectin (FC) test kits have been widely used (Mosli et al., 2015). Although FC test kits offer a simple and convenient assessment, this method cannot provide accurate information about the IBD location or its stage (Lehmann et al., 2015). Additionally, the level of different biomarkers highly depends on several factors, such as patients' diet and water content in fecal samples (Lehmann et al., 2015). This presents a need for techniques for more direct monitoring throughout the GI tract and evaluation of the progress of the disease with therapeutic. Direct monitoring methods can be classified into probe-based and capsule-based methods. While probe-based endoscopy is the gold standard test for the upper GI tract (Goetz, 2018), this method is invasive and does not provide access to monitor the lower part of the GI tract (Voderholzer et al., 2005). Owing to the miniaturization of electronics and advancements in imaging technologies in the last two decades, video capsule endoscopy (VCE) has revolutionized our ability to noninvasively monitor regions of the GI tract that were previously inaccessible (Ahmed, 2022). However, imaging techniques are still expensive and error-prone due to their subjective nature and lack of proper quantitative metrics (Rosenkrantz et al., 2015). As a result, early detection of IBD is not guaranteed using these techniques, as visual markers might not be prevalent in the early stages of inflammation.

Moreover, an expert technician is required to interpret the visual data, rendering this approach unsuitable for frequent monitoring (Rosenkrantz et al., 2015). As an alternative, more objective and quantitative methods that use biomarkers (Gopalakrishnan et al., 2023; Waimin et al., 2022)as indicators of intestinal and systemic inflammation have been of great interest to the scientific and medical community (Nejati et al., 2021; Waimin et al., 2020). To achieve this, Mimee et al. reported a capsule that combined photoluminescent bacteria with a miniaturized wireless readout to produce a minimally invasive device capable of in-vivo biosensing (Mimee et al., 2018). Although this capsule provides high specificity, the complexity, and risk involved in introducing living gene-manipulated microorganisms into the human body pose limitations to this approach. Another alternative is capsule-based platforms with integrated gas sensors. Kourosh Kalantar-Zadeh et al. reported a capsule that detects carbon dioxide ($CO_2$) and other gases and provides information about the gut microbiome's general health (Kalantar-Zadeh et al., 2017). However, $CO_2$ is an indirect

indicator of IBD and cannot confidently reflect the inflammation status. Hence, a need exists to integrate direct inflammation biomarkers sensors into such platforms.

While MPO and Calprotectin are well-known direct biomarkers of inflammation used in the fecal analysis, their detection methods involve the use of antigen-antibody for their detection, which limits them to single-use diagnostics applications and cannot be designed into sensors for continuous profiling throughout the GI tract. As an alternative, ROS has been identified as a unique biomarker often linked to elevated levels of inflammation (Bourgonje et al., 2020) which can be directly assessed by monitoring the Oxidation Reduction Potential (ORP) levels in the environment using more robust electrochemical sensors (Saha et al., 2023). Miniaturization and integration of such ORP sensors can allow an in-situ platform for continuously monitoring and detecting regions of inflammation with elevated levels of ROS throughout the GI tract.

To address this need, we have designed and developed a capsule with a simple onboard ORP sensor for detecting inflammation and a pH sensor for tracking the capsule's location throughout the GI tract. This platform combines wireless low-power potentiometric readout units, optimized to last for 48 h, with cost-effective materials to provide real-time assessment of potential lesions of inflammation throughout the GI tract. The simplicity of the design, in conjunction with the optimal power consumption, makes our smart capsules suitable for frequent in-situ monitoring through the GI tract over a long period which in turn improves therapeutic efficacy and helps early detection of potential risks of relapses in IBD patients. Similar to other smart capsule technologies, such as the well-known PillCam™ by Medtronic, the developed capsule is intended for single-use applications and follows the same administration and expulsion process. Once the capsule is ingested, it follows the natural peristaltic motion of the GI tract and is eventually expelled through the body's normal defecation process.

## 2. Materials and methods

### 2.1. Working principle

As illustrated in Fig. 1, the GI tract consists of the mouth, stomach, small intestine, and large intestine (McQuilken, 2021), each presenting a distinct luminal pH level (Nejati et al., 2022) and capsule transit time (Koziolek et al., 2015). The pH level in the mouth varies between pH 5 and pH 8. However, it reduces to pH 2–3 in the stomach due to the secretion of acids, such as HCl, necessary for digestion. The overall transit time for a capsule in the stomach can reach up to 6 h. As the capsule transitions to the beginning of the small intestine, the luminal pH level increases to pH 6, followed by a gradual increase reaching approximately pH 7.4 at the terminal ileum with an average transit time of 2–6 h. Subsequently, in the cecum, the pH level drops below pH 6 and then rises again to a pH of 6.7 at the rectum with a transit time varying between 6 and 70 h. This unique feature of the luminal pH profile throughout the GI tract allows the utilization of a pH-sensitive potentiometric sensor to convert the luminal pH values to potential readings to track the location of the administered capsule at different time points as it passes throughout the GI tract. It should also be noted that while there may be some variability between patients due to factors such as diet and diseases, the distinct changes in pH levels between the stomach and the small intestine and

between the small intestine and the large intestine are often recognized as markers of the capsule's transition and entry into a different organ section.

In addition to the distinct pH levels, the small intestine and colon present a plethora of microbiomes responsible for the digestion and metabolism of food and are particularly important for assessing inflammation in IBD patients. Since 90% of the microbiome in the small and large intestines are anaerobic bacterial species, the ORP level, under normal circumstances in these regions, exhibits a low redox potential (Rigottier-Gois, 2013). However, with an increase in inflammation, there is a buildup of reactive oxygen species in response to the deregulated recruitment of neutrophils to the site of inflammation (Lakhan and Kirchgessner, 2010). Therefore, in patients with IBD, the elevated ROS levels lead to an increase in the redox potential at the site of inflammation.

The integration of pH and ORP sensors within a smart ingestible capsule offers valuable insights into the location of inflammation within the GI tract. It should be also noteworthy that precise localization of inflammation may be challenging solely based on pH measurements. However, by combining the information obtained from the distinct pH changes and the gradual change in the pH profile throughout the small intestine and large intestine, one can still obtain valuable information about the approximate position of the capsule within these segments. This information can provide rough estimates, indicating whether the capsule is in the beginning, central, or end portion of each segment (e.g., small intestine or large intestine). To realize this integrated system, the pH and ORP sensing platforms were implemented using low-power electronics and zero-powered potentiometric measurement modalities. The working electrodes of the pH and ORP sensors were comprised of ion-selective electrodes (ISE) placed on the cap of the capsule exposed to the environment while internally connected to potentiometric interfaces inside the capsule. In order to provide more effective miniaturization/integration of the sensors on the capsule surface, a common reference electrode was realized on the cap of the capsule using Ag/AgCl to provide a shared reference potential to both pH and ORP sensors. (Bakker et al., 2008) (Baltsavias et al., 2020). In accordance with the potentiometric equations (Refer to *Equations* in Supporting Information), the wireless potentiometric platform utilizes the pH potential ($V_{pH}$) to track the capsule's position in the GI tract. The ORP values ($V_{ORP}$) are used to analyze GI health. In a healthy person, low levels of ROS activity in the colon translate to a stable and low level of ORP readings. However, in conditions where inflammation has occurred, a surge in ROS levels at the site of inflammation results in an increase in $V_{ORP}$ levels in a localized fashion based on Eq. 3. Therefore, a significant spike in the ORP levels in the wireless readout unit reflects elevated levels of ROS activity which can be utilized to identify regions of inflammation throughout the GI tract.

## 2.2. Fabrication of capsule with integrated electrochemical sensors

The capsule housing was designed using Autodesk® Inventor with an inner diameter, outer diameter, and external height of 9, 11, and 22 mm, respectively. The cap and the body of the capsule were 3D printed separately using the stereolithography method (Form 3 by Formlabs Inc.) (Gopalakrishnan et al., 2022b). After the 3D printing process, all components were rinsed with pure isopropyl alcohol (IPA) and ultraviolet (UV) photocured for 15

min at 60 °C. The cap of the capsule consisted of three compartments for pH, ORP, and reference electrodes (Fig. 2a(i)). Each compartment was designed with feed-through wire connectors for electrical connection between the electrodes and internal electronics inside the capsule. After attaching the feed through copper wires, the designated compartments of the pH and ORP working electrodes were filled with Graphite conductive paste (Dupont 7102) (Krishnakumar et al., 2022b; Mishra et al., 2022; Sedaghat et al., 2019), and the compartment of the common reference electrode was filled with Ag/AgCl conductive paste (Dupont 5880) (Heredia Rivera et al., 2022; Heredia-Rivera et al., 2022a) as illustrated in Fig. 2a(ii). The coated pastes were cured in an oven at 100 °C for 10 min (Zareei et al., 2021, 2022). While one of the bare carbon electrodes was used as an ORP measurement electrode without further treatment to prepare the reference and pH electrodes, the Ag/AgCl electrode (Heredia-Rivera et al., 2022b) and the other carbon electrodes were coated with a solid electrolyte coating (Fig. 2a(iii) and a pH-sensitive membrane (Fig. 2a(iv)), respectively (Sedaghat et al., 2020, 2021). The solid electrolyte coating was made by mixing fine potassium chloride (KCl) particles, polyvinyl chloride (PVC, P/N 81387, high molecular weight), and cyclohexanone with a weight ratio of 1:1:7. The pH-sensitive membrane mixture was made by adding 1.5 wt% of H-ionophore (II), 65 wt% of o-NPOE, 0.5 wt % Sodium tetrakis [3,5-bis(trifluoromethyl) phenyl]borate Selectophore (NaTFPB, MilliporeSigma) and 33 wt% PVC (high molecular weight) to 3 mL of tetrahydrofuran (THF). All coated membranes were left to dry overnight under ambient conditions. Three printed circuit boards (PCB) (each of diameter 8 mm) were designed, manufactured, and assembled for interfacing the pH sensor and ORP sensor with a microcontroller unit (MCU) (Fig. 2a(v)) (Kasi et al., 2023). Batteries of diameter 8 mm were integrated along with a normally closed reed switch for magnetic activation of the capsule (Fig. 2a(vi)). Next, the PCBs were connected in the following order from the top of the capsule – buffer circuit for ORP sensor, buffer circuit for pH sensor, and the control unit, with the sensors at the top of the capsule and the battery unit below the three PCBs. A common reference electrode and individual working electrodes from the respective sensors are connected to both buffer circuits. The outputs of the two buffer circuits were connected to the analog pins of the microcontroller unit (MCU) on the PCB. Power of 1.8 V and ground were supplied to the buffer circuits from the voltage regulator circuit in the control unit PCB. The magnetic reed switch was connected between the positive terminal of the battery and the printed circuit board with the control unit. The electronic components were enclosed within the body of the capsule (Fig. 2a(viii)) by screwing the two compartments (cap and body) of the capsule together. In order to provide effective water-tightness of the assembled capsule a small amount (<20 μl) of silicone adhesive (3M 5200 Marine Sealant) was applied to the screw features on the capsule prior to full assembly. To validate the effective water-tightness of the capsule assembly process, a series of tests were conducted (Refer to *Water-tightness test* in Supporting Information) as shown in Fig. S1. Once the capsule was tightly screwed, the magnet was attached to the body of the capsule, deactivating the internal electronics until the designated testing time point. Fig. 2b shows the photograph of the various electronic components along with the 3D-printed cap and body parts of the capsule prior to the full assembly. Fig. 2c(i) depicts a photograph of the fully assembled capsule with the magnet securely attached to its body. The activation process of the internal electronics within the capsule and the subsequent data communication to the receiver is accomplished by simply

removing the magnet from the side wall of the capsule enabling a switching mechanism (Gopalakrishnan et al., 2017), as illustrated in Fig. 2c(ii).

### 2.3. Preparation of pH and ORP standard solutions

To simulate the pH and redox potential levels of different parts of the GI tract and evaluate the performance of the sensors, representative standard solutions were prepared. pH buffer solutions with standard pH values ranging from 1.2 to 8.0 were created by accurately mixing specific amounts of potassium chloride, hydrochloric acid, potassium hydrogen phthalate, potassium hydrogen phosphate (monobasic), and sodium hydroxide (all chemicals were purchased from MilliporeSigma) in deionized (DI) water. The chemicals were added in calculated quantities to achieve the desired pH values. Prior to each experiment, the pH levels of all solutions were meticulously monitored using a commercial pH probe coupled with a Hach data acquisition system (Hach, USA). This ensured accurate and consistent pH measurements throughout the study. The highly oxidizing standard solutions with an ORP level of 600 mV (labeled as Sol. 1 throughout this study) were purchased from MilliporeSigma. Solutions with ORP level of 469 mV (at 25 °C), also known as Light's solution, were prepared by dissolving 3.92 g of ferrous ammonium sulfate (MilliporeSigma), and 4.82 g of ferric ammonium sulfate (MilliporeSigma) in 100 mL of DI water acidified with 5.6 mL of sulfuric acid (MilliporeSigma) and labeled as Sol. 2 throughout this study. ZoBell's ORP/Redox standard solution (227 mV, 25 °C) was purchased from Hach Co. (Colorado, USA) and labeled as Sol. 3 throughout this study. For the preparation of the reducing solutions based on quinhydrone, first, phosphate buffer solution (PBS, pH = 7) was made by dissolving the calculated amounts of potassium dihydrogen phosphate (MilliporeSigma) and anhydrous disodium hydrogen phosphate (Mallinckrodt Co, UK) in 1 L DI water. Then, a stock ORP standard solution with a nominal potential of 86 mV (at °25 C) was prepared by dissolving 10 g of quinhydrone within 1L of that PBS, which was labeled as Sol. 4 throughout this study. The highly reducing ORP standard solutions (with nominal potentials of −50 mV (Sol. 5), −250 mV (Sol. 6), −450 mV (Sol. 7), and −550 mV (Sol. 8) at room temperature) were prepared via controlled addition of 1 mM NaOH to 200 mL of the previously prepared Sol. 4 stock solution.

### 2.4. Cell culture studies

To validate the increase in the ORP levels and to correlate it to an ongoing inflammatory response, in-vitro studies were performed using the Human Leukemia cell line (HL-60) procured from the American Type Culture Collection (ATCC) Cell Culture Line (CCL-240). The HL-60 cells were used as a model to trigger the inflammation process as they can easily be differentiated into neutrophils, a primary immune cell encountered in IBD-related diseases. The cells were cultured in Iscove's Modified Dulbecco's Media (IMDM)/F-12 media containing 10% Fetal Bovine Serum (FBS), 100 U/ml penicillin, and 100 μg/ml streptomycin with 5% Carbon Dioxide ($CO_2$) at a 37 °C humidified incubator in a T75 flask. The cells were passed every 72 h, and the concentration was maintained at $5 \times 10^5$ cells/ml within each pass (counted using countess cell counter, Invitrogen, Thermo Fisher Scientific, Massachusetts, USA). Then, the cell lines were differentiated into neutrophils by adding 1 μL of 10 mM All-Trans Retinoic Acid (ATRA) in the culture media without penicillin and streptomycin and were incubated for 7 days. Following the formation of neutrophils,

to mimic the neutrophil invasion and overall immune system response artificially, the cells were treated with phorbol 12-myristate 13-acetate (PMA). For this process, the cells were seeded into a 24-culture plate, and PMA was administered to the cells inside an anaerobic chamber to generate similar physiological conditions in the GI tract. To simulate low and high levels of inflammation, two concentrations of PMA (90 nM and 180 nM) were added to the culture plates seeded with the cells alongside an untreated control as a baseline. As a validation for the induction of inflammation with PMA, conventional inflammatory biomarkers such as MPO and Calprotectin levels were analyzed using a quantitative MPO Activity Assay kit procured from EnzChek, Thermo fisher (Massachusetts, USA) and Calprotectin levels using BÜHLMANN fCAL® ELISA (New Hampshire, USA). The ORP levels after inducing the inflammation were measured using a commercial Hach probe and the integrated electronic capsule to quantify the increase in ROS levels.

## 3. Results and discussion

### 3.1. Design of electronics

The electronic unit of the smart capsule is composed of three printed circuit boards (PCBs), two 1.5 V button cell batteries, an RF antenna, and a reed switch, as shown in the exploded view of the capsule (Fig. 3a). The control unit is realized on the first PCB and is composed of a microcontroller, a voltage regulator circuit, and a crystal oscillator. The microcontroller used is an nRF52832 MCU for its exceptionally low energy consumption (nRF52832), which collects the data from the electrochemical sensors and facilitates wireless communication between the capsule and the portable external receiver (Gopalakrishnan et al., 2021, 2022a). Potentiometric electrochemical sensors, such as pH and ORP sensors, are characterized by extremely high source impedance ($10^5$–$10^{12}\Omega$) (Light, 1997). This high impedance arises from the nature of the sensing mechanism, necessitating minimal current drawn from the sensors to ensure accurate and long-term stable measurements (CAMMANN and XIE, 1989; Saha et al., 2022). Therefore, to minimize the current drawn from developed pH and ORP sensors on the capsule, high-impedance buffer circuits were used as an interface between sensors and the MCU. Inset in Fig. 3a shows the schematic of the buffer circuit designed using Op-Amps in a double-stage unity-gain configuration all of which were assembled on a single PCB unit. Texas Instruments OPA373 Op-Amp, chosen for providing a high input impedance with considerably low input bias current, which operated at a bias voltage of 1.8 V (OPAx373) and regulated by an Analog Devices' LT6656 (LT6656). Two buffer circuits were realized on the second and third PCBs for interfacing pH and ORP sensors with the MCU. Fig. 3b illustrates the block-level architecture of the communication system employed in the smart capsule. The RF antenna was specifically designed for transmission within the frequency range of 2.40 GHz–2.50 GHz, which corresponds to Bluetooth communication. Rigorous RF characterizations were conducted, demonstrating the electronic unit's capability to maintain reliable and stable data transmission at a frequency of 2.49 GHz in both air and liquid environments (refer to Supporting Information Fig. S2). The capsule utilizes Bluetooth communication protocol to periodically transmit data to the base station, which is based on a Raspberry Pi platform. This base station serves as a receiver for the transmitted data. To facilitate further analysis and visualization by healthcare professionals, the collected data is

then transferred from the base station to a computer of choice through the integrated Wi-Fi communication module (refer to Supporting Information Fig. S3).

### 3.2. ISE interface circuit analysis

Two analyses were conducted to evaluate the performance of the ISE buffer circuit interface utilized in the integrated capsule platform. The first test aimed to determine the linear operating range of the buffer circuit, while the second test assessed the stability of the circuit at high input impedance. To simulate the behavior of the ISE, the electrical equivalent of the sensor was modeled as a signal generator acting as a voltage source connected in series with a high resistance (Fig. 3c). The output of this circuit was connected to the designed buffer circuit. The signal generator was connected between the $V_{working}$ and $V_{ref}$ pins on the PCB, mimicking the input voltage from the sensors. The input voltage was varied from −2V to +2V to cover a wide range of operating conditions. The output of the buffer circuit was measured for different input resistance values (1 MΩ, 100 MΩ, and 1000 MΩ) using a potentiometer. The measurements were plotted as a function of the differential input voltage (Fig. 3d). The results demonstrated that the buffer circuit exhibited high linearity within the range of −1V to +1V, which corresponds well to the expected voltage range produced by the two ISE (pH and ORP sensors) used in the capsule design. Furthermore, Fig. 3e illustrates the stability of the buffer circuit in the high-impedance mode of sensing. The plot shows minimal fluctuations within the linear operating range, even for input resistances on the order of 1 GΩ. This observation suggests that the designed buffer circuit interface effectively maintains its performance in the typical resistance range of many ISEs.

### 3.3. Power management

To ensure efficient power management and uninterrupted operation of the capsule throughout the entire GI tract while maintaining appropriate data sampling rates and resolution, a systematic power consumption analysis was conducted on the fully integrated capsule. As data transmission is a significant power-consuming aspect during remote monitoring, the study aimed to investigate the impact of data transmission rate, determined by the data sampling frequency, on the capsule's operational lifespan (Fig. 3f). The data sampling frequency was varied from 15 Hz to 800 Hz, and the current drawn from the power supply was measured. The results revealed an idle current consumption of 2.5 mA during standby mode (without data communication), while peak current consumption ranged from 5.0 mA to 8.0 mA during data transmission, irrespective of the data transmission rate (Fig. 3g). By analyzing the current waveforms obtained for each data sampling frequency, the energy consumption rate of the capsule was calculated and plotted (Fig. 3h). Considering the integrated battery capacity of 150 mAh, the findings indicated that lower sampling frequencies (15 Hz) provided an operational lifespan of 60 h. However, operating the capsule at higher sampling rates (800 Hz) significantly reduced the battery life to less than 20 h. Considering the average GI transit time of 48 h for the capsule to traverse from the mouth to the end of the colon (Kinget and Kalala, 2009), the optimal sampling frequency was determined to be 60 Hz. This frequency allowed for high-resolution data sampling while effectively preserving battery life during the capsule's transit throughout the GI tract.

### 3.4. Performance of pH sensor

To test the performance of the electrochemical sensors, the integrated pH on the capsule cap was placed in different buffer solutions with pH values varying from 1.2 to 8.0, and the generated potential was measured using the developed miniaturized readout unit and commercial potentiostat (Lawson Labs, Inc.) for ground truth readings. The capsule was retained in each solution for 10 min and subsequently moved to the next solution in the order from lower to higher pH and then back to lower values of pH, Fig. 4a. Fig. 4b shows the resulting potentiometric response of the pH sensors with two readout units. It can be observed that the miniaturized readout unit shows less than ±5 mV difference from the commercial potentiostat, indicating the combined stability of the sensor and readout unit. The calibration curve shows an average linear sensitivity ($r^2$ = 0.9925) of −43.2 mV/pH with great repeatability performance, Fig. 4c. Sensor stability and drift are of major concern in many electrochemical sensors. Therefore, the long-term stability of the sensors with the miniaturized readout unit was tested by placing the pH sensor in solutions of pH values 1.25, 5.00, and 8.00 while continuously recording output potential for 24 h. The results of these tests showed a stable output voltage with less than ±4 mV drifts over the 24 h test, Fig. 4d. These results further confirm the high stability of the pH sensor and readout unit for practical implementation within the physiologically relevant range of the GI tract.

### 3.5. Performance of ORP sensor

To verify the performance of the ORP sensor, the integrated ISE sensors on the capsule cap were placed in standard ORP solutions varying from −400 mV to +625 mV. The capsule was placed in each solution for 10 min and subsequently moved to the next solution. The experimental setup was similar to that of the pH performance tests. In this case, the output potential of the ORP sensor was continuously recorded using the designed portable read-out unit and commercial potentiostat, Fig. 4e. Fig. 4g shows the output potential measurements of the ORP sensor in response to increasing and decreasing levels of ORP using both readout units. The sensor exhibits distinct potential change at each ORP level with a fast response time of 25 s and less than ±4 mV difference between the two measurement readout units, Fig. 4f. The readings from the ORP sensors with the portable readout unit show an overall low hysteresis and good linear sensitivity with a correlation coefficient $r^2$ = 0.974 across the ORP range of −400 mV to +625 mV, Fig. 4g. To test the long-term stability of the electrodes, the ORP sensor was placed in different ORP solutions for 24 h while continuously recording the output potential using the developed portable readout unit. As observed, the output values stayed relatively constant with a minimal deviation of less than ±4.2 mV over 24 h, which was significantly smaller than the potential levels of each solution.

### 3.6. In vitro characterization of integrated capsule

To evaluate the capability of the fully integrated capsule to measure and wirelessly transmit both pH and ORP data simultaneously, two in vitro scenarios were created to simulate a healthy and inflamed GI tract. For the healthy GI tract simulation, four solutions were prepared with pH values of 5.5, 3.5, 6.0, and 6.7, representing the pH levels inside the mouth, stomach, small intestine, and colon, respectively. The corresponding ORP values of

each solution were 100 mV, 400 mV, 100 mV, and −50 mV, reflecting the ROS levels in the respective organs (Fig. 5a). These solutions were used to mimic the movement of the capsule through the various organs of the healthy GI tract (Fig. 5b(i)). To simulate inflamed conditions in the small GI tract, the solution representing the small intestinal condition was modified. Instead of having an ORP value of 100 mV, it was replaced with a higher ORP value of 550 mV while maintaining the pH value of 6.0 (Fig. 5a). The integrated capsule was sequentially placed in each of the prepared solutions to imitate its movement through the organs of the inflamed GI tract (Fig. 5b (ii)). The potential values measured by the integrated capsule were remotely recorded using the portable external reader. These recorded values were then converted to corresponding pH and ORP levels of the respective gut environments, providing insights into the pH and oxidative stress levels in both healthy and inflamed conditions.

The results obtained from the studies demonstrate the high accuracy of the wirelessly collected pH measurements, with a relative standard deviation (RSD) of 3.33% and a negligible ΔpH of 0.2 compared to the ground truth values (Fig. 5c). Similarly, the ORP measurements also exhibited accurate readings for the healthy GI tract, with an RSD of 1.20% and a ΔORP of less than 5 mV relative to the ground truth readings (Fig. 5d). These findings further validate the reliability and robustness of the remote monitoring approach.

Notably, in the artificially simulated inflammation scenario in the small intestine, the integrated capsule detected a significant increase of approximately 450 mV in the ORP level compared to the healthy simulating condition (Fig. 5d). This observation confirms the ability of the integrated system for remote monitoring and assessment of pH and ORP levels in gut-like environments, facilitating effective GI health monitoring. In order to further validate the performance and accuracy of our integrated pH and ORP sensors in the complex environment of the GI tract, a series of experiments were conducted with the capsule in GI fluid (Figs. S4a and S4b) that was freshly collected from the cecum section of the pig models (Refer to *GI fluid test* in Supporting Information). As observed in Figs. S4c and S4d, the integrated sensors demonstrated high accuracy (±1.010% error for pH and ±2.419% error for ORP), and stability (negligible drift of <0.050/h for pH and <−0.466 mV/h for ORP), which were comparable to the results obtained from the commercial probes. Furthermore, to validate the biocompatibility of all the materials used in the construction of the capsule and use in ingestible applications, a series of in vitro tests were conducted (Refer to *Biocompatibility Assessment* in Supporting Information). As observed in Fig. S5, all the constituents of the capsule and sensing electrodes demonstrated cell viability of >80% indicating high levels of biocompatibility.

### 3.7. Cellular inflammation assessment with integrated capsule

The pathogenesis of inflammation in IBD involves various cellular and molecular processes, including the deregulation of T-cells, overexpression of proinflammatory biomarkers, and increased activity of neutrophils at the site of inflammation. Neutrophils play a crucial role in IBD inflammation by forming NETs and releasing MPO-mediated ROS in a process known as NETosis (Fig. 6a). To validate the formation of ROS and the subsequent increase

in ORP levels in a physiologically relevant gut environment, in vitro studies were conducted using differentiated neutrophils under anaerobic conditions.

The inflammation induction process and changes in ORP levels in the culture environment were assessed using standard inflammation monitoring kits and a commercial ORP monitoring probe. Differentiated neutrophils were treated with two different concentrations of PMA, namely 90 nM and 180 nM, and the inflammation process was validated by measuring the levels of MPO and Calprotectin (Fig. 6b). The levels of MPO and calprotectin were observed to increase by approximately 6.0 ng/mL and 0.2 ng/mL, respectively, with a PMA concentration of 180 nM, confirming the induction of inflammation. In contrast, a PMA concentration of 90 nM showed low expression of MPO and calprotectin levels, consistent with previous studies that observed significant NETs formation only at PMA concentrations above 100 nM (Smith et al., 1998). ORP levels were measured using a commercial probe to validate the use of ORP as an effective marker of inflammation. Fig. 6c demonstrates the recorded changes in ORP levels in the culture media upon exposing neutrophils to 90 nM and 180 nM of PMA. An increase of 60 mV in ORP levels was observed with a PMA concentration of 90 nM, while a higher increase of 120 mV was observed with 180 nM of PMA. The cells without PMA exposure showed no noticeable change in ORP levels, confirming the potential use of ORP levels as an effective biomarker to differentiate between healthy and inflamed tissue conditions.

Subsequently, the integrated capsule was tested to evaluate its ability to detect the risk of inflammation in physiologically relevant conditions. The fully assembled capsule was placed in a 6-well plate containing differentiated neutrophils and culture media and placed in an aerobic chamber (Fig. 6d(i)). pH and ORP levels in the culture media were wirelessly recorded and demonstrated a stable pH value of 7.5 with negligible changes in ORP levels prior to the introduction of PMA into the culture media. However, upon the addition of 100 nM PMA into the culture media, a clear increase in ORP levels of approximately 70 mV was observed (Fig. 6d(ii) & 6e), while the pH value remained unaffected (with a fluctuation of approximately 7.30% in readings). These results were consistent with the previous findings using the commercial ORP probe. The observed results further validate the ability of the integrated capsule to monitor pH reliably and remotely and ORP levels within the area of interest, making it an effective platform for assessing potential risks and inflammation lesions throughout the GI tract.

## 4. Conclusions

IBD has become a critically important global disease due to its increasing prevalence around the world. The rampant cases of IBD are exacerbated by the elevated rates of relapses reported among patients in remission, which necessitates frequent monitoring of the GI health of patients using easily accessible and inexpensive medical tools. To address this need, we have designed and developed a smart capsule with integrated pH and ORP sensors to track the capsule’s location and measure inflammation-indicative ROS levels throughout the GI tract. The capsule’s performance was validated through in vitro studies, demonstrating its ability to differentiate between healthy and inflamed conditions in the GI tract. By optimizing the wireless transmission capabilities, we ensured continuous

monitoring of pH and ORP levels during the capsule's passage through the GI tract within the expected transit time (48 h). Furthermore, in a cell culture medium simulating the GI environment, the capsule successfully detected and recorded increased ORP levels upon the introduction of inflammation. This capsule represents a promising approach to overcome the limitations of current invasive monitoring methods for IBD. By providing non-invasive, frequent monitoring, it has the potential to reduce the risk of relapses and improve therapeutic management. Moving forward, in vivo studies with animal models will be crucial to validate the performance and clinical utility of the capsule prior to its use in clinical studies involving human subjects. Further advancements of the platform must involve exploring the possibility of creating capsules with more rounded surfaces, edges, and more compact sizes to minimize discomfort during swallowing and transit through the GI tract.

## Supplementary Material

Refer to Web version on PubMed Central for supplementary material.

## Acknowledgments

Funding for this research was provided in part by Eli Lilly Strategic Partnership, the School of Materials Engineering at Purdue University, National Institute of Diabetes and Digestive and Kidney Diseases program at National Institutes of Health (IR21DK128715-01A1) and National Institute of Food and Agriculture (13699514). The authors would also like to acknowledge the support staff and engineers of Birck Nanotechnology Center, School of Electrical and Computer Engineering, and School of Materials Engineering at Purdue University.

## Data availability

Data will be made available on request.

## References

Ahmed M, 2022. Video capsule endoscopy in gastroenterology. Gastroenterol. Res. 15, 47. 10.14740/GR1487.

Alatab S, et al. , 2020. The global, regional, and national burden of inflammatory bowel disease in 195 countries and territories, 1990–2017: a systematic analysis for the Global Burden of Disease Study 2017. Lancet Gastroenterol. Hepatol. 5, 17–30. 10.1016/S2468-1253(19)30333-4. [PubMed: 31648971]

Ananthakrishnan AN, 2015. Epidemiology and risk factors for IBD. Nat. Rev. Gastroenterol. Hepatol. 2015 12 (4 12), 205–217. 10.1038/nrgastro.2015.34.

Bakker E, Bhakthavatsalam V, Gemene KL, 2008. Beyond potentiometry: robust electrochemical ion sensor concepts in view of remote chemical sensing. Talanta 75, 629–635. 10.1016/J.TALANTA.2007.10.021. [PubMed: 18585124]

Baltsavias S, van Treuren W, Weber MJ, Charthad J, Baker S, Sonnenburg JL, Arbabian A, 2020. In vivo wireless sensors for gut microbiome redox monitoring. IEEE Trans. Biomed. Eng. 67, 1821–1830. 10.1109/TBME.2019.2948575. [PubMed: 31634824]

Bourgonje AR, Feelisch M, Faber KN, Pasch A, Dijkstra G, van Goor H, 2020. Oxidative stress and redox-modulating therapeutics in inflammatory bowel disease. Trends Mol. Med. 26, 1034–1046. 10.1016/J.MOLMED.2020.06.006. [PubMed: 32620502]

Brinkmann V, Reichard U, Goosmann C, Fauler B, Uhlemann Y, Weiss DS, Weinrauch Y, Zychlinsky A, 2004. Neutrophil extracellular traps kill bacteria. Science (1979) 303, 1532–1535. 10.1126/SCIENCE.1092385/SUPPL_FILE/BRINKMANN.SOM.PDF.

Cammann K, Xie SL, 1989. ISE selectivity and ION-exchange kinetics. Ion-Selective Electrodes 43–64. 10.1016/B978-0-08-037933-3.50008-9.

Coskun M, 2014. Intestinal epithelium in inflammatory bowel disease. Front. Med 1 10.3389/FMED.2014.00024.

Digestive diseases: MedlinePlus medical Encyclopedia [WWW Document], n.d. URL. https://medlineplus.gov/ency/article/007447.htm. (Accessed 19 January 2023).

Goetz M, 2018. Endoscopic surveillance in inflammatory bowel disease. Visc. Med. 34, 66. 10.1159/000485019. [PubMed: 29594172]

Gopalakrishnan S, DasGupta A, Nair DR, 2017. Novel RF MEMS capacitive switches with design flexibility for multi-frequency operation. J. Micromech. Microeng. 27, 095013 10.1088/1361-6439/AA7D21.

Gopalakrishnan S, Nejati S, Sedaghat S, Gupta K, Mishra RK, Rahimi R, 2023. Electronic-free and low-cost wireless sensor tag for monitoring fish freshness. Sensor. Actuator. B Chem. 381, 133398 10.1016/J.SNB.2023.133398.

Gopalakrishnan S, Sedaghat S, Krishnakumar A, He Z, Wang H, Rahimi R, 2022a. Wireless humidity sensor for smart packaging via one-step laser-induced patterning and nanoparticle formation on metallized paper. Adv. Electron. Mater. 10.1002/AELM.202101149.

Gopalakrishnan S, Waimin J, Raghunathan N, Bagchi S, Shakouri A, Rahimi R, 2021. Battery-less wireless chipless sensor tag for subsoil moisture monitoring. IEEE Sensor. J. 21, 6071–6082. 10.1109/JSEN.2020.3039363.

Gopalakrishnan S, Waimin J, Zareei A, Sedaghat S, Raghunathan N, Shakouri A, Rahimi R, 2022b. A biodegradable chipless sensor for wireless subsoil health monitoring. Sci. Rep. 12, 1–14. 10.1038/s41598-022-12162-z, 2022 12:1. [PubMed: 34992227]

Heredia Rivera U, Kadian S, Nejati S, White J, Sedaghat S, Mutlu Z, Rahimi R, 2022. Printed low-cost PEDOT:PSS/PVA polymer composite for radiation sterilization monitoring. ACS Sens. 7, 960–971. 10.1021/ACSSENSORS.1C02105/SUPPL_FILE/SE1C02105_SI_001.PDF. [PubMed: 35333058]

Heredia-Rivera U, Gopalakrishnan S, Kadian S, Nejati S, Kasi V, Rahimi R, 2022a. A wireless chipless printed sensor tag for real-time radiation sterilization monitoring. J. Mater. Chem. C Mater 10, 9813–9822. 10.1039/D2TC00531J.

Heredia-Rivera U, Kasi V, Krishnakumar A, Kadian S, Barui AK, He Z, Wang H, Stanciu L, Rahimi R, 2022b. Cold atmospheric plasma-assisted direct deposition of polypyrrole-Ag nanocomposites for flexible electronic sensors. ACS Appl. Mater. Interfaces 15. 10.1021/ACSAMI.2C20798/ASSET/IMAGES/LARGE/AM2C20798_0010 (JPEG).

Jain S, 2011. Treatment of inflammatory bowel disease (IBD). Pharmacol. Rep. 63, 629–642. [PubMed: 21857074]

Kalantar-Zadeh K, Ha N, Ou JZ, Berean KJ, 2017. Ingestible sensors. ACS Sens. 2, 468–483. 10.1021/ACSSENSORS.7B00045/ASSET/IMAGES/LARGE/SE-2017-000458_0007 (JPEG). [PubMed: 28723186]

Kasi V, Zareei A, Gopalakrishnan S, Alcaraz AM, Joshi S, Arfaei B, Rahimi R, 2023. Flexible hybrid electronics via near-infrared radiation-assisted soldering of surface mount devices on screen printed circuits. Adv. Electron. Mater. 9, 2201012 10.1002/AELM.202201012.

Kinget R, Kalala W, 2009. Liesbeth vervoort & guy van den mooter (1998) colonic drug targeting. J. Drug Target. 6, 129–149. 10.3109/10611869808997888.

Koziolek M, Grimm M, Becker D, Iordanov V, Zou H, Shimizu J, Wanke C, Garbacz G, Weitschies W, 2015. Investigation of pH and temperature profiles in the GI tract of fasted human subjects using the Intellicap® system. J. Pharmaceut. Sci. 104, 2855–2863. 10.1002/JPS.24274.

Krishnakumar A, Kadian S, Heredia Rivera U, Chittiboyina S, Lelièvre SA, Rahimi R, 2022a. Organ-on-a-Chip platform with an integrated screen-printed electrode array for real-time monitoring trans-epithelial barrier and bubble formation. ACS Biomater. Sci. Eng. 10.1021/ACSBIOMATERIALS.2C00494/ASSET/IMAGES/LARGE/AB2C00494_0008 (JPEG).

Krishnakumar A, Mishra RK, Kadian S, Zareei A, Rivera UH, Rahimi R, 2022b. Printed graphene-based electrochemical sensor with integrated paper microfluidics for rapid lidocaine detection in blood. Anal. Chim. Acta 1229, 340332. 10.1016/J.ACA.2022.340332. [PubMed: 36156230]

Lakhan SE, Kirchgessner A, 2010. Neuroinflammation in inflammatory bowel disease. J. Neuroinflammation 7, 37. 10.1186/1742-2094-7-37. [PubMed: 20615234]

Lechuga S, Ivanov AI, 2017. Disruption of the epithelial barrier during intestinal inflammation: quest for new molecules and mechanisms. Biochim. Biophys. Acta 1864, 1183. 10.1016/J.BBAMCR.2017.03.007.

Lehmann FS, Burri E, Beglinger C, 2015. The role and utility of faecal markers in inflammatory bowel disease. Therap. Adv. Gastroenterol. 8, 23. 10.1177/1756283X14553384.

Light TS, 1997. Industrial use and applications of ion selective electrodes. J. Chem. Educ. 74, 171–177. 10.1021/ED074P171.

LT6656 Datasheet and Product Info | analog devices. [WWW Document], URL https://www.analog.com/en/products/lt6656.html. (Accessed 19 January 2023).

McQuilken SA, 2021. The mouth, stomach and intestines. Anaesth. Intensive Care Med. 22, 330–335. 10.1016/J.MPAIC.2021.04.001.

Mimee M, Nadeau P, Hayward A, Carim S, Flanagan S, Jerger L, Collins J, McDonnell S, Swartwout R, Citorik RJ, Bulović V, Langer R, Traverso G, Chandrakasan AP, Lu TK, 2018. An ingestible bacterial-electronic system to monitor gastrointestinal health. Science 360, 915. 10.1126/SCIENCE.AAS9315. [PubMed: 29798884]

Mishra RK, Krishnakumar A, Zareei A, Heredia-Rivera U, Rahimi R, 2022. Electrochemical sensor for rapid detection of fentanyl using laser-induced porous carbon-electrodes. Microchim. Acta 189, 1–11. 10.1007/S00604-022-05299-1/METRICS.

Mosli MH, Zou G, Garg SK, Feagan SG, MacDonald JK, Chande N, Sandborn WJ, Feagan BG, 2015. C-reactive protein, fecal calprotectin, and stool lactoferrin for detection of endoscopic activity in symptomatic inflammatory bowel disease patients: a systematic review and meta-analysis. Am. J. Gastroenterol. 110, 802–819. 10.1038/AJG.2015.120. [PubMed: 25964225]

Nejati S, Wang J, Heredia-Rivera U, Sedaghat S, Woodhouse I, Johnson JS, Verma M, Rahimi R, 2021. Small intestinal sampling capsule for inflammatory bowel disease type detection and management. Lab Chip 22, 57–70. 10.1039/D1LC00451D. [PubMed: 34826326]

Nejati S, Wang J, Sedaghat S, Balog NK, Long AM, Rivera UH, Kasi V, Park K, Johnson JS, Verma MS, Rahimi R, 2022. Smart capsule for targeted proximal colon microbiome sampling. Acta Biomater. 154, 83–96. 10.1016/J.ACTBIO.2022.09.050. [PubMed: 36162763]

nRF52832 - Versatile Bluetooth 5.2 SoC - nordicsemi.com. [WWW Document], URL https://www.nordicsemi.com/products/nrf52832. (Accessed 19 January 2023).

Rigottier-Gois L, 2013. Dysbiosis in inflammatory bowel diseases: the oxygen hypothesis microbe-microbe and microbe-host interactions. ISME J. 7, 1256–1261. 10.1038/ismej.2013.80. [PubMed: 23677008]

Roda G, Chien Ng S, Kotze PG, Argollo M, Panaccione R, Spinelli A, Kaser A, Peyrin-Biroulet L, Danese S, 2020. Crohn's disease. Nat. Rev. Dis. Primers 2020 6, 1–19. 10.1038/s41572-020-0156-2, 1 6.

Rosales C, 2018. Neutrophil: a cell with many roles in inflammation or several cell types? Front. Physiol 9, 113. 10.3389/FPHYS.2018.00113/BIBTEX. [PubMed: 29515456]

Rosenkrantz AB, Mendiratta-Lala M, Bartholmai BJ, Ganeshan D, Abramson RG, Burton KR, Yu JPJ, Scalzetti EM, Yankeelov TE, Subramaniam RM, Lenchik L, 2015. Clinical utility of quantitative imaging. Acad. Radiol. 22, 33. 10.1016/J.ACRA.2014.08.011. [PubMed: 25442800]

Saha A, Sedaghat S, Gopalakrishnan S, Waimin J, Yermembetova A, Glassmaker N, Mousoulis C, Shakouri A, Wei A, Rahimi R, Alam MA, 2023. A new paradigm of reliable sensing with field-deployed electrochemical sensors integrating data redundancy and source credibility. Scientific Reports 2023 13, 1–13. 10.1038/s41598-022-25920-w, 1 13.

Saha A, Yermembetova A, Mi Y, Gopalakrishnan S, Sedaghat S, Waimin J, Wang P, Glassmaker N, Mousoulis C, Raghunathan N, Bagchi S, Rahimi R, Shakouri A, Wei A, Alam MA, 2022. Temperature self-calibration of always-on, field-deployed ion-selective electrodes based on differential voltage measurement. ACS Sens. 7, 2661–2670. 10.1021/ACSSENSORS.2C01163/SUPPL_FILE/SE2C01163_SI_001.PDF. [PubMed: 36074898]

Santiago M, Stocker F, Ministro P, Gonçalves R, Carvalho D, Portela F, Correia L, Lago P, Trindade E, Dias CC, Magro F, 2022. Incidence trends of inflammatory bowel disease in a southern

European country: a mirror of the western world? Clin. Transl. Gastroenterol. 13, e00481 10.14309/CTG.0000000000000481. [PubMed: 35347090]

Sedaghat S, Jeong S, Zareei A, Peana S, Glassmaker N, Rahimi R, 2019. Development of a nickel oxide/oxyhydroxide-modified printed carbon electrode as an all solid-state sensor for potentiometric phosphate detection. New J. Chem. 43, 18619–18628. 10.1039/C9NJ04502C.

Sedaghat S, Nejati S, Bermejo LH, He Z, Alcaraz AM, Roth A, Li Z, Pol VG, Wang H, Rahimi R, 2021. Laser-induced atmospheric CuxO formation on copper surface with enhanced electrochemical performance for non-enzymatic glucose sensing. J. Mater. Chem. C Mater 9, 14997–15010. 10.1039/D1TC01289D.

Sedaghat S, Piepenburg CR, Zareei A, Qi Z, Peana S, Wang H, Rahimi R, 2020. Laser-Induced mesoporous nickel oxide as a highly sensitive nonenzymatic glucose sensor. ACS Appl. Nano Mater. 3, 5260–5270. 10.1021/ACSANM.0C00659/SUPPL_FILE/AN0C00659_SI_001.PDF.

Smith ME, Van Maesen, Der K, Somera FP, Sobel RA, 1998. Effects of phorbol myristate acetate (PMA) on functions of macrophages and microglia in vitro. Neurochem. Res. 23, 427–434. 10.1023/A:1022478005243/METRICS. [PubMed: 9482257]

Instruments Texas, 2003. OPAx373, OPAx374 6.5-MHz, 585-μA, rail-to-rail I/O CMOS operational amplifier Revised Sept. 2016) [WWW Document], URL. https://www.ti.com/lit/ds/symlink/opa373.pdf?ts=1674179916347. (Accessed 19 January 2023).

Voderholzer WA, Beinhoelzl J, Rogalla P, Murrer S, Schachschal G, Lochs H, 2005. Small bowel involvement in Crohn's disease: a prospective comparison of wireless capsule endoscopy and computed tomography enteroclysis. INFLAMMATORY BOWEL DISEASE Gut 54, 369–373. 10.1136/gut.2004.040055. [PubMed: 15710985]

Waimin J, Gopalakrishnan S, Heredia-Rivera U, Kerr NA, Nejati S, Gallina NLF, Bhunia AK, Rahimi R, 2022. Low-cost nonreversible electronic-free wireless pH sensor for spoilage detection in packaged meat products. ACS Appl. Mater. Interfaces 14, 45752–45764. 10.1021/ACSAMI.2C09265/SUPPL_FILE/AM2C09265_SI_001.PDF. [PubMed: 36173396]

Waimin JF, Nejati S, Jiang H, Qiu J, Wang J, Verma MS, Rahimi R, 2020. Smart capsule for non-invasive sampling and studying of the gastrointestinal microbiome. RSC Adv. 10, 16313–16322. 10.1039/C9RA10986B. [PubMed: 35498852]

Zareei A, Gopalakrishnan S, Mutlu Z, He Z, Peana S, Wang H, Rahimi R, 2021. Highly conductive copper-silver bimodal paste for low-cost printed electronics. ACS Appl. Electron. Mater. 3 10.1021/acsaelm.1c00345.

Zareei A, Selvamani V, Gopalakrishnan S, Kadian S, Maruthamuthu MK, He Z, Nguyen J, Wang H, Rahimi R, 2022. A biodegradable hybrid micro/nano conductive zinc paste for paper-based flexible bioelectronics. Adv. Mater. Technol. 7, 2101722 10.1002/ADMT.202101722.

Zhang B, Gulati A, Alipour O, Shao L, 2020. Relapse from deep remission after therapeutic de-escalation in inflammatory bowel disease: a systematic review and meta-analysis. J. Crohns Colitis. 14, 1413. 10.1093/ECCO-JCC/JJAA087. [PubMed: 32335670]

Zhu H, Li YR, 2012. Minireview Oxidative stress and redox signaling mechanisms of inflammatory bowel disease: updated experimental and clinical evidence. Exp. Biol. Med. 237, 474–480. 10.1258/ebm.2011.011358.

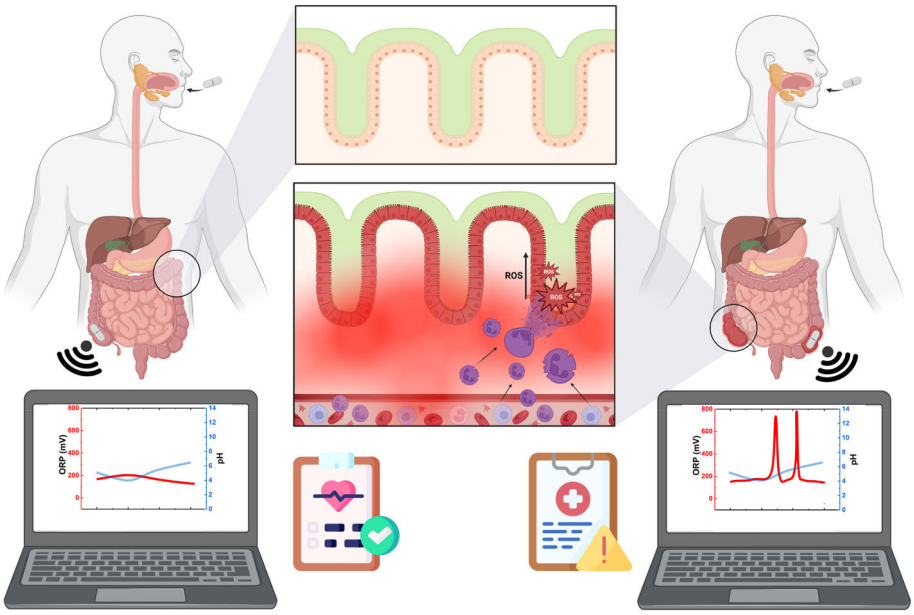


**Fig. 1.**

Conceptual illustration of a healthy and inflamed GI tract and the working principle of the wireless smart capsule in measuring the pH and ORP levels corresponding to the location of the capsule and ROS levels in the GI tract, respectively.

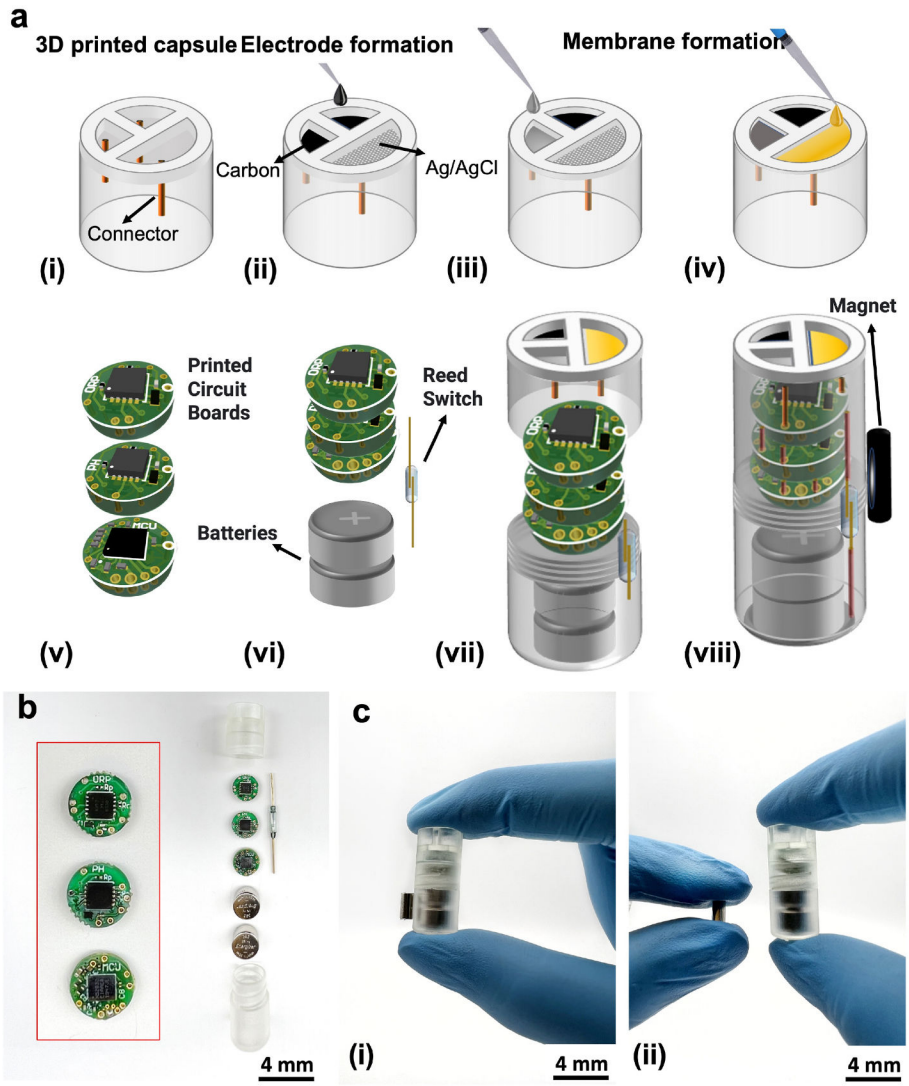


**Fig. 2.**

Fabrication process of the Smart capsule (a) (i) 3D printing of the capsule housing with sensor connectors. (ii) Carbon paste dispensing in two compartments and Ag/AgCl paste dispensing in one compartment followed by oven drying. (iii) pH-sensitive membrane coating on pH sensor working electrode and oven drying. (iv) Solid electrolyte coating on Ag/AgCl electrode and oven drying. (v) Fabrication three PCBs including two buffer circuit interfaces for pH and ORP measurements and one PCB with MCU data connection and communication. (vi) Assembly of three PCBs with batteries and reed switch. (vii) Placement of the electronic components into the 3D printed capsule and connection to pH and ORP sensors. (viii) Placement of external magnet to the body of the capsule deactivate the reed switch and powering of the integrated electronics. (b) Photograph of the all-electronic components used in the capsule. (c) (i) Photograph of the fully integrated capsule with the magnet in place to deactivate the device when not in use. (ii) The capsule is activation and data communication are achieved by removing the magnet with a small force.

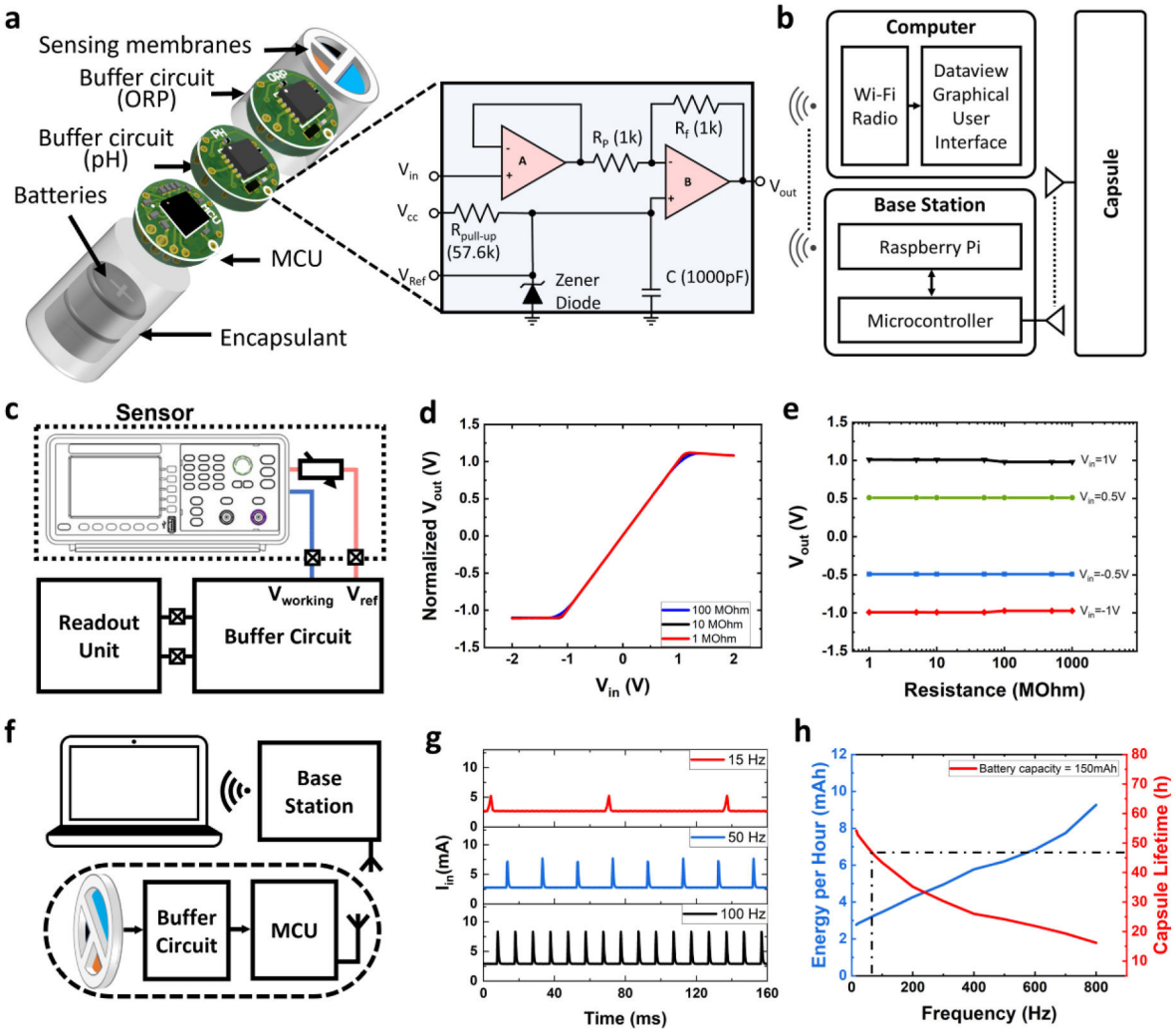


**Fig. 3.**

Design and characterization of the electronic modules of the capsule. (a) Exploded view of the capsule with the electronic components. Inset illustrates the circuit diagram of the ISE interface. (b) Block level architecture of the communication system between the capsule and the reader. (c) Schematic of the experimental setup to assess the performance of the ISE interface circuit using an electrical equivalent circuit of the sensor and an external readout unit. (d) The output voltage of the buffer circuit plotted as a function of the input voltage for various values of series resistance demonstrating the linearity and working range of the potentiometric readings. (e) The output voltage of the buffer circuit plotted as a function of the series resistance demonstrating the stability of the circuit to varying internal resistances of the ISE. (f) Schematic of the test setup to determine the power consumption capsule electronics at different data transmission rates. (g) Current measurements from the power source at different data transmission rate. (h) Average energy consumption and lifetime of the capsules plotted as a function of measurement and data transmission frequency.

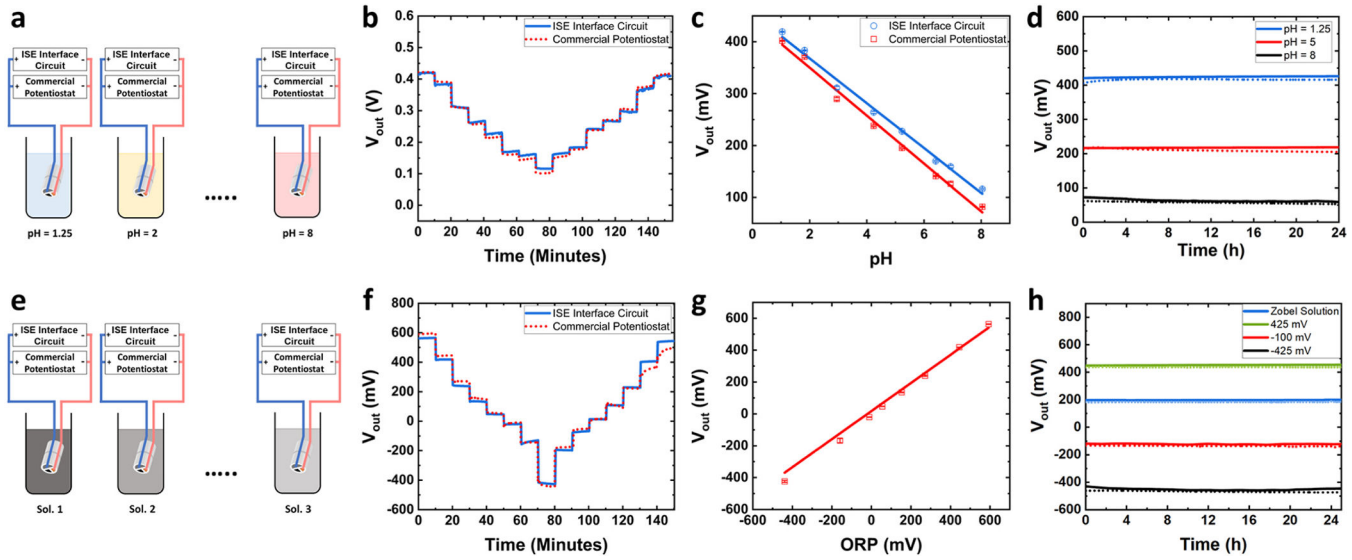


**Fig. 4.**

Assessment of pH and ORP sensors with interface readout circuit. (a) Schematic illustration of the experimental setup used to characterize the developed pH sensor in various pH solutions with measurements using the developed miniaturized electronics and a standard commercial potentiostat. (b) The measured output voltage of the pH sensor in various pH solutions as a function of time. (c) Calibration curve for the pH sensor collected using miniaturized electronics (RSD = 0.967%) and a standard commercial potentiostat (RSD = 0.865%). (d) Long-term stability measurements of the pH sensor with miniaturized readout electronics. (e) Schematic illustration of the experimental setup used to characterize the developed ORP sensor in various ORP solutions with measurements using the developed miniaturized electronics and a standard commercial potentiostat. (f) The measured output voltage of the ORP sensor in various ORP solutions as a function of time. (g) Calibration curve for the integrated ORP sensor (RSD = 3.650%). (h) Long-term stability ORP sensors with miniaturized readout electronics.

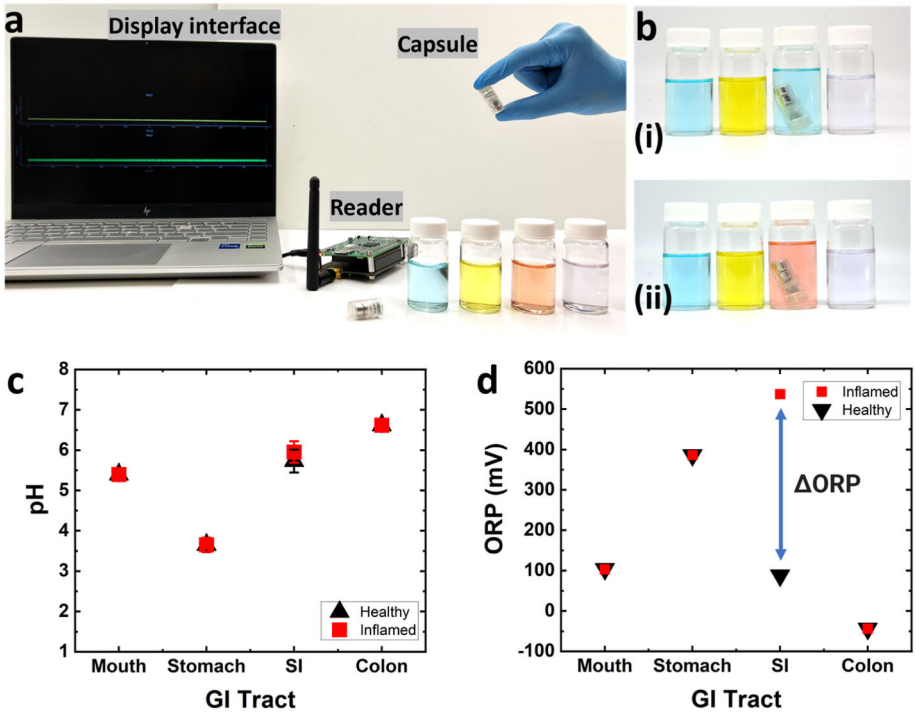


**Fig. 5.**

In vitro characterization of a fully assembled capsule with pH and ORP sensors. (a) Photograph of the experimental setup for in-vitro characterization of the integrated capsule with the external reader and display interface. (b) Photograph of four solutions prepared to simulate the pH and ORP levels in the mouth, stomach, small intestine, and colon in (i) healthy and (ii) inflamed conditions in the small intestine. (c) pH levels measured by the smart capsule in four solutions acting as a surrogate for various organs of the GI tract. (d) ORP levels measured by the smart capsule in four solutions representing healthy and inflamed GI tract conditions. A spike in ORP level is observed at the simulated site of inflammation.

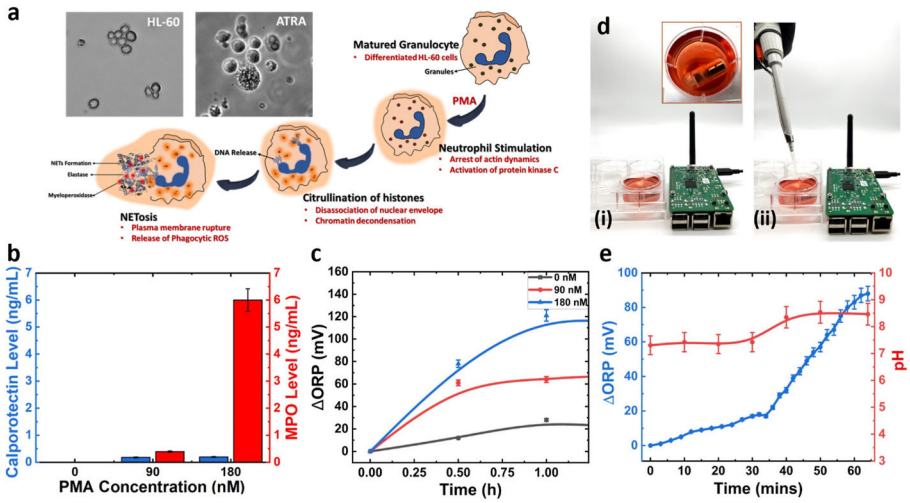


**Fig. 6.**

Assessment of capsule performance in a simulated gut environment with cellular inflammation. (a) Schematic illustration of various stages of cellular inflammation in IBD conditions. (b) Calprotectin and MPO levels as a function of the concentration of PMA introduced in the differentiated neutrophils cells culture. (c) Change in ORP level of culture media after introducing various PMA concentrations (RSD = 4.20%). (d) Photograph of the capsule placed inside a well plate containing neutrophils cells (i) before and (ii) after the introduction of PMA while continuously recording pH and ORP levels through the external reader. (e) Measured ΔORP and pH with the smart capsule before and after introducing PMA into the neutrophils cell culture media (RSD = 4.78%).